nature climate change

SUPPLEMENTARY INFORMATION

DOI: 10.1038/NCLIMATE1932

Anthropogenic impact on Earth's hydrological cycle

The models used in the analysis are listed in Table S1. The table also provides information on the ensemble size of the two experiments with all forcings (ALL) and greenhouse gas emissions only (GHG), as well as the length of the control simulation.

Table S1. Details of the 8 CMIP5 models used in this study

Model	ALL ensemble size	GHG ensemble size	Length of Control
CCSM4	6	3	500
CNRM-CM5	10	6	850
CSIRO-Mk3-6-0	10	5	500
CanESM2	5	5	995
GFDL-CM3	5	3	500
GISS-E2-H	5	5	240,240
GISS-E2-R	5	5	300,500
HadGEM2-ES	4	4	1030

Timeseries of the annual mean northern hemisphere land precipitation are illustrated in Fig. S1. Model simulations with all forcings agree better with the observations than simulations with GHG forcings only. The latter show an increase in precipitation throughout the period considered here and become consistent with the observations only after the 1980s. The inclusion of the remaining forcings leads to a decrease in precipitation in the early part of the period, with the exception of the CCSM4 model which, however, does not represent the indirect effect of the aerosol forcing that may be key to understanding the early change. Our optimal fingerprinting analysis with CCSM4 yields high uncertainties in the scaling factors which can be explained by the fact that the model does not capture the decrease in precipitation in the early decades and that recent years, when the signal intensifies, are not included in the simulations. Patterns of the post-1950s grid-point trends produced with the observations and model simulations with all forcings are shown in Fig. S2. The model patterns correspond to the ensemble mean of the ALL simulations and are therefore smoother than the observed trend patterns. The models indicate negative trends in regions with higher aerosol emissions. The observed patterns are less uniform and show higher trends, but are also more influenced by the effect of internal variability.

DOI: 10.1038/NCLIMATE1932

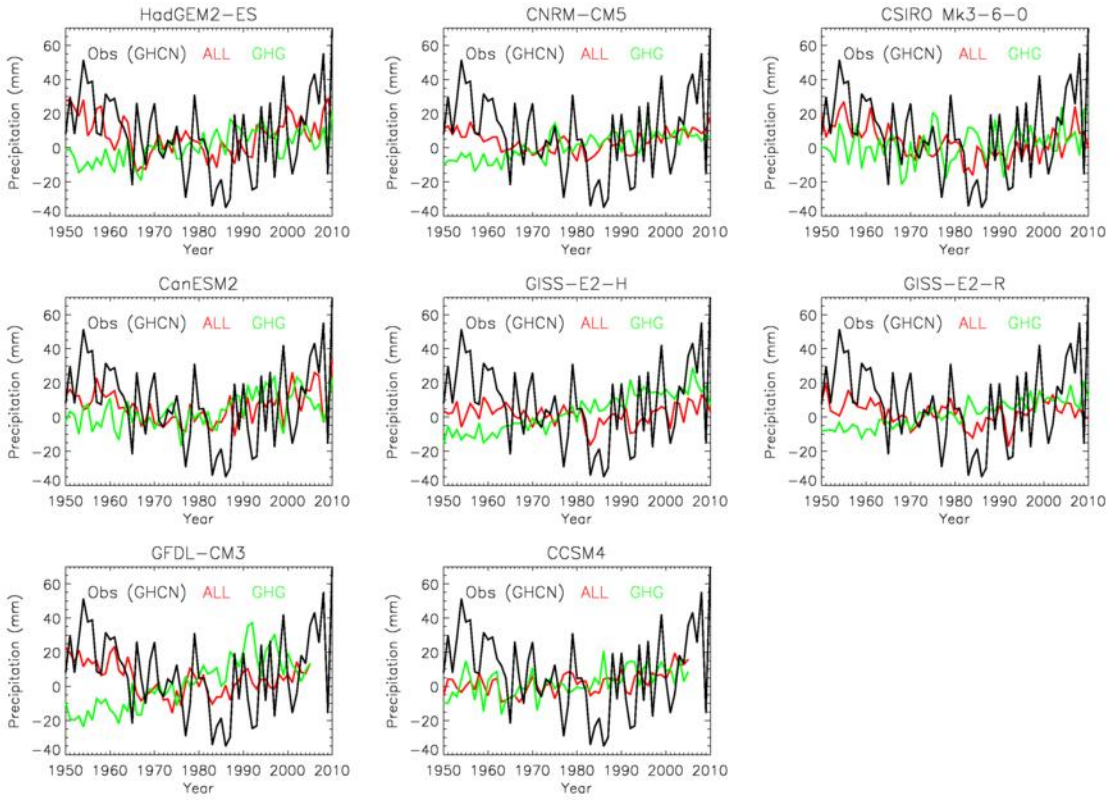

Figure S1 Timeseries of the annual mean northern hemisphere land precipitation since 1950 estimated using GHCN observations (black line) and model data from simulations that include all forcings (red lines) and the greenhouse gas forcing only (green lines). The precipitation estimates are shown as anomalies relative to the 1961-1990 mean. An individual figure panel is shown for each of the models employed in this study. The ALL and GHG timeseries are constructed using the ensemble mean of the corresponding model experiment.

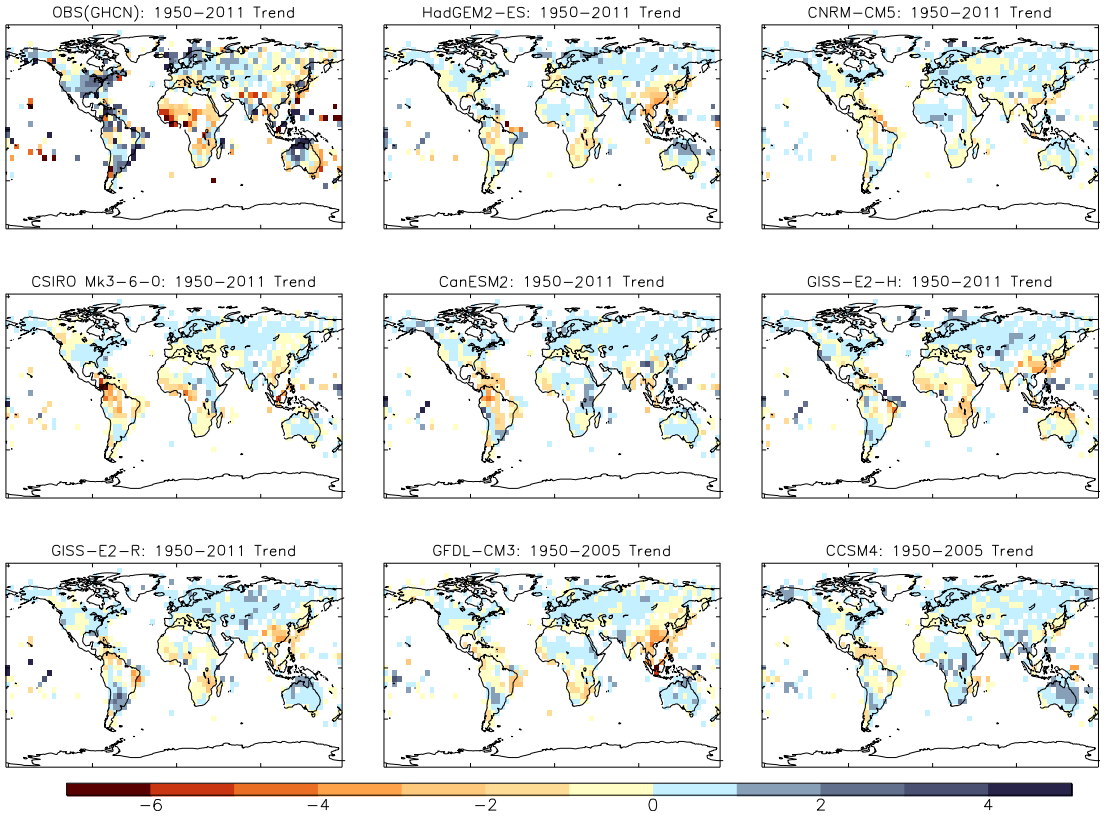

Figure S2 Land precipitation trends since 1950 (in units of mm/year). The different panels show the trends computed from GHCN observations and from each of the models used in this study. The modelled trends correspond to the ensemble mean of the simulations with all forcings.

DOI: 10.1038/NCLIMATE1932

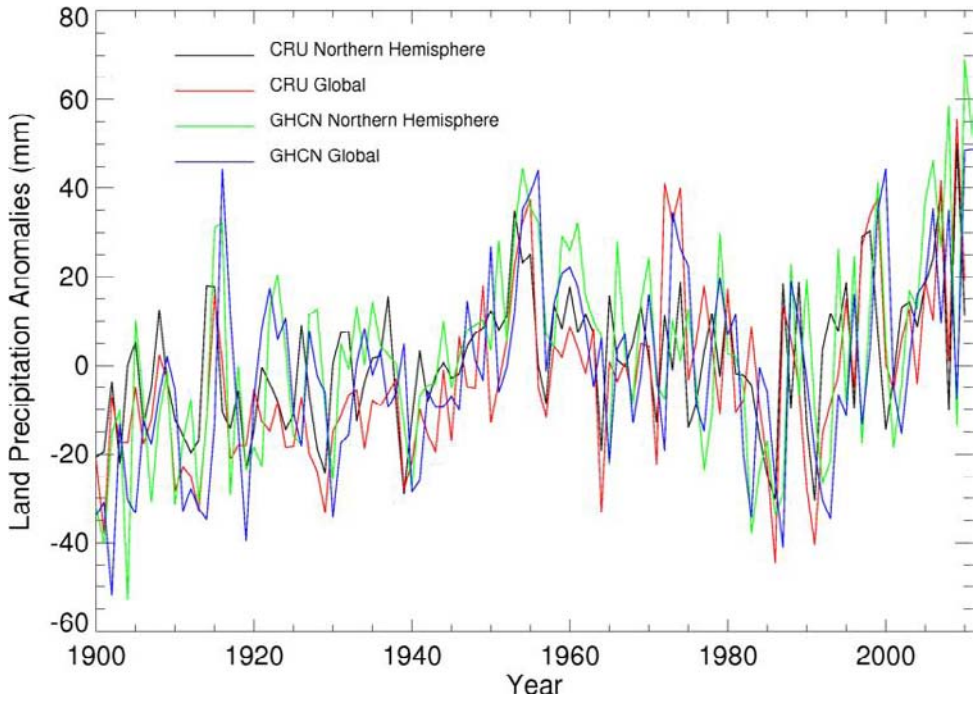

Figure S3 Comparison of northern hemisphere land mean precipitation with global land mean precipitation in GHCN and CRU datasets. CRU data are normalized with reference to the period 1961-1990 to be consistent with GHCN data.